

Individual Assembly of Two-Species Rydberg Molecules Using Optical Tweezers

Alexander Guttridge^{1,2,*} Tom R. Hepworth^{1,2} Daniel K. Ruttley^{1,2}

Aileen A. T. Durst³ Matthew T. Eiles³ and Simon L. Cornish^{1,2}

¹*Department of Physics, Durham University, South Road, Durham, DH1 3LE, United Kingdom*

²*Joint Quantum Centre Durham-Newcastle, Durham University, South Road, Durham, DH1 3LE, United Kingdom*

³*Max Planck Institute for the Physics of Complex Systems, Nöthnitzer Straße 38, 01187 Dresden, Germany*



(Received 19 December 2024; accepted 13 March 2025; published 3 April 2025)

We present a new approach to investigating Rydberg molecules by demonstrating the formation and characterization of individual Rb*Cs Rydberg molecules using optical tweezers. By employing single-atom detection of Rb and Cs, we observe molecule formation via correlated loss of both species and study the formation dynamics with single-particle resolution. We control the interatomic distances by manipulating the relative wave function of atom pairs using the tweezer intensity, optimizing the coupling to molecular states and exploring the effect of the tweezer on these states. Additionally, we demonstrate molecule association with atoms trapped in separate tweezers, paving the way for state-selective assembly of polyatomic molecules. The observed binding energies, molecular alignment, and bond lengths are in good agreement with theory. Our approach is broadly applicable to Rydberg tweezer platforms, expanding the range of available molecular systems and enabling the integration of Rydberg molecules into existing quantum science platforms.

DOI: 10.1103/PhysRevLett.134.133401

Understanding and controlling molecules at the quantum level is a fundamental goal in both atomic physics and quantum chemistry, with broad implications for quantum technologies such as quantum simulation, precision measurement, and quantum computation [1,2]. Ultracold molecules provide an excellent platform for investigating molecular phenomena, as their ultralow temperatures enable precise control and delicate probing of quantum states [3]. Rydberg molecules, in particular, exhibit several unique features originating from their exaggerated bond lengths that extend to micrometer scales. This makes them ideal for exploring molecular behavior on macroscopic scales.

Several different types of Rydberg molecules have been experimentally explored, including ultralong-range Rydberg molecules (ULRMs) [4–6], where a Rydberg electron binds to a ground-state atom, and Rydberg macrodimers [7–9], which are bound states of two Rydberg atoms. While Rydberg molecules have been successfully created in optical lattices [9–11], the overwhelming majority of experimental work, including recent studies of heteronuclear species [12,13], has been conducted in bulk gases using ion detection methods. These methods limit the precise control and

detection of individual molecules [14]. Such capabilities are highly desirable—and often essential—for realizing theoretical proposals that leverage interactions between Rydberg and ground-state atoms to produce heavy Rydberg states [15,16], for quantum information processing [17], and to study electron dynamics, including localization and topological behavior, in highly structured microscopic environments [18–20].

Optical tweezer arrays have emerged as a versatile tool for trapping, controlling, and detecting individual atoms with exceptional precision [21]. The interparticle distances in tweezer arrays closely match the bond lengths of Rydberg molecules, offering the possibility of studying these states with single-particle sensitivity. The recent development of two-species tweezer arrays [22–24] introduces independent control over each species, enabling applications such as the assembly of ground-state diatomic molecules [25,26] and the realization of promising new platforms for quantum computing [27,28]. These advancements lay the groundwork for realizing ULRMs in tweezers using a two-species approach.

In this Letter, we demonstrate the creation of individual Rb*Cs ULRMs using an optical tweezer platform. By employing single-atom detection of Rb and Cs, we observe ULRM formation by correlated loss of both species and leverage the single-particle resolution to study the formation dynamics. We characterize the influence of the tweezers on molecule formation, optimizing coupling to the molecular state by manipulating the relative wave function of the atom pair. Additionally, we demonstrate

*Contact author: alexander.guttridge@durham.ac.uk

Published by the American Physical Society under the terms of the [Creative Commons Attribution 4.0 International license](https://creativecommons.org/licenses/by/4.0/). Further distribution of this work must maintain attribution to the author(s) and the published article's title, journal citation, and DOI.

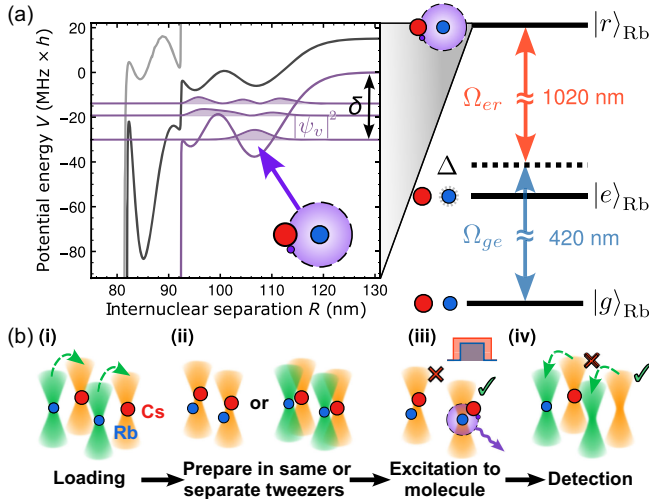


FIG. 1. (a) Relevant energy levels for excitation of ULRMs. Right: two-photon Rydberg excitation scheme for Rb atoms. The ground state $|g\rangle_{\text{Rb}}$ is coupled to the Rydberg state $|r\rangle_{\text{Rb}}$ via an off-resonant intermediate state $|e\rangle_{\text{Rb}}$, with detuning Δ from $|g\rangle_{\text{Rb}} \rightarrow |e\rangle_{\text{Rb}}$. Left: experimentally relevant PECs of the Rb^*Cs system as a function of internuclear separation R . The curves are colored according to their asymptotic quantum numbers: $|36S, m_j = -1/2, m_f = 3\rangle$ (purple) and $|36S, m_j = 1/2, m_f = 2\rangle$ (black). The gray PEC does not support bound states in the relevant energy region. Molecular states are supported by these PECs, with vibrational wave functions ψ_v (purple) shown for $|36S, m_j = -1/2, m_f = 3\rangle$. The two-photon detuning δ is defined with respect to the atomic transition. (b) Experimental scheme for production and detection of Rb^*Cs ULRMs in tweezers. (i) Rb and Cs atoms are loaded into separate tweezers and Rb atoms are moved toward the Cs tweezers. (ii) Rb and Cs atoms are prepared either in the same tweezer or in separate tweezers. (iii) The atom pair is illuminated with Rydberg light to photoassociate a ULRM. (iv) Rb and Cs are separated into their respective tweezers and detected. Molecule formation results in loss of the atom pair.

the association of molecules with each atom trapped in separate tweezers, allowing precise control over the interatomic distance.

We investigate ULRMs formed from a ground-state ^{133}Cs atom and a Rydberg ^{87}Rb atom. The excited valence electron of the Rb atom interacts strongly with the Cs atom when the internuclear separation R is smaller than the Rydberg orbit. This interaction is characterized by the low-energy S - and P -wave electron-Cs scattering phase shifts [29,30]. Exemplary Born-Oppenheimer potential energy curves (PECs) are shown in Fig. 1(a). At large R , where the interatomic interactions are negligible compared to the Zeeman splitting, these curves are labeled by the Rydberg electron's magnetic quantum number m_j and the quantum number m_f of the ground-state Cs atom; the lower purple (upper black) curve has $m_j = -1/2$ and $m_f = 3$ ($m_j = 1/2$ and $m_f = 2$). Only the lower curve is experimentally accessible for our choice of initial atomic states; the upper

curves are accessible only via state mixing through the electron-Cs interaction. Molecular states, with binding energy E_v and vibrational wave functions ψ_v , are supported by potential wells in the oscillatory structure of these curves. These oscillations are directly linked to the fluctuating electronic density spatially probed by the Cs atom [29], while the nearly vertical steps at ~ 82 and 92 nm stem from the low-energy 3P_J -wave shape resonances of Cs^- [31–33]. The calculation includes both fine and hyperfine structure and the Zeeman interaction with the external magnetic field [34–36]. The calculation is benchmarked at zero magnetic field using an alternative method based on the Coulomb Green's function [37]. Additionally, we use scattering phase shifts incorporating minor adjustments determined by previous measurements of Cs^- photodetachment cross sections [33] and Cs^*Cs photoassociation spectroscopy [38,39].

To prepare ULRMs in tweezers we follow the protocol in Fig. 1(b). Each experiment begins with single Rb and Cs atoms in the motional ground state of species-specific tweezers [39]. To prepare the Rb + Cs atom pair at the required separation, we merge an 817 nm tweezer containing a Rb atom into a 1066 nm tweezer containing a Cs atom. Depending on the experiment, we either maintain the tweezers at a fixed separation or prepare both atoms in the 1066 nm tweezer by adiabatically reducing the 817 nm tweezer intensity. Using the two-photon excitation scheme shown in Fig. 1(a), we excite the Rb + Cs atom pair to a Rb^*Cs ULRM. After excitation, we separate any remaining atoms into their respective tweezers. We take atomic fluorescence images at the start and end of each sequence to determine each tweezer's occupancy.

Figure 2 shows spectroscopy of a Rb^*Cs ULRM in tweezers. We first investigate molecular states below the atomic state $|36S_{1/2}, m_j = -1/2\rangle_{\text{Rb}}$ (PEC shown in Fig. 1), with the Rb + Cs atom pair prepared in the same 1066 nm tweezer. We scan the Rydberg laser frequency below the atomic state and measure the probability of losing a Rb or Cs atom. Nondestructive imaging of Rb and Cs atoms in separate tweezers before excitation allows postselection for cases with only an Rb atom [Fig. 2(a)] or an Rb + Cs pair [Fig. 2(b)] initially present.

For the Rb-only case, we observe a single loss peak corresponding to the atomic line. This loss occurs because Rydberg atoms are antitrapped at our tweezer wavelength. The contrast of this peak is limited by the likelihood that a Rydberg atom decays before escaping the tweezer; most decay events populate another hyperfine state of the ground manifold, which does not couple to our Rydberg lasers. The 150 μs excitation pulse saturates the atomic transition, leading to significant broadening.

In Fig. 2(b) the blue markers show events where we detect only the loss of the Rb atom and keep the Cs atom, showing a similar peak around the atomic line. Additionally, the purple markers reveal extra peaks corresponding to the loss of both atoms from the tweezers, indicating Rb^*Cs ULRM

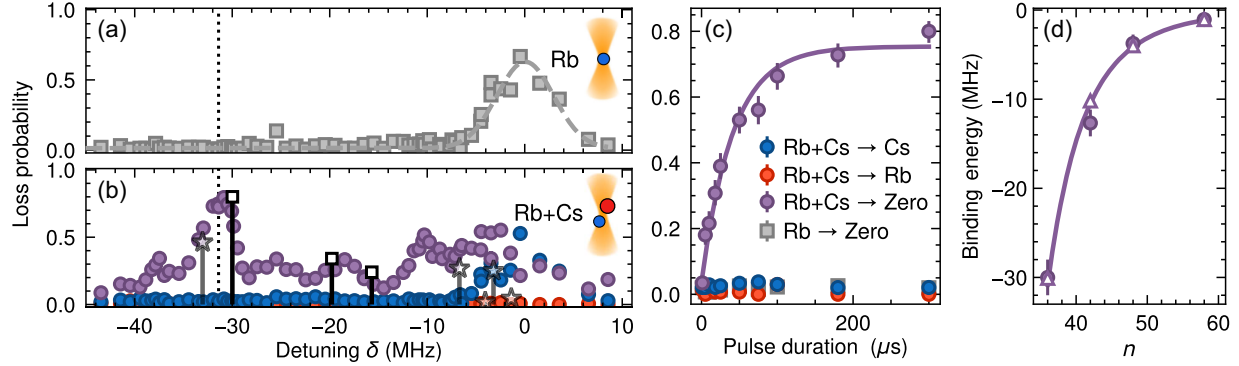


FIG. 2. (a),(b) Spectroscopy of (a) individual Rb atoms and (b) Rb+Cs pairs in a magnetic field of 4.78 G and tweezer intensity of $I = 93 \text{ kW/cm}^2$ as a function of the detuning δ from the atomic state $|36S_{1/2}, m_j = -1/2\rangle_{\text{Rb}}$. We show the probability of losing an individual Rb atom (gray squares) with a Gaussian fit (gray dashed line) to extract the atomic line position. For atom pairs, the loss probabilities of both atoms (purple), Cs atom (red), or Rb atom (blue) are shown with theoretical predictions for molecular line positions and strengths (black squares). Star-shaped markers with lighter shading indicate bound states that are highly sensitive to the P -wave phase shift. (c) Loss probabilities as a function of the duration of the Rydberg pulse with detuning $\delta = -31.4 \text{ MHz}$ [vertical dotted line in (a) and (b)]. (d) Binding energy of $v = 0$ states for $nS \text{ Rb}^* \text{Cs}$ ULRMs as a function of principle quantum number n . The filled circles (empty triangles) show the measured (predicted) binding energies and the line shows a power-law fit to the data.

formation. We assign states to molecular peaks by comparing their positions to theoretical calculations [39]. The stick spectrum locations indicate theoretical line positions, with heights showing expected line strengths. These strengths incorporate electronic transition strengths and vibrational Franck-Condon factors (FCFs). We assign the strongest peak around $\delta = -31 \text{ MHz}$ as the $v = 0$ state. The black lines correspond to the three vibrational levels in Fig. 1(a), whose energies are insensitive to the 3P_0 shape resonance position. In contrast, the lighter shading indicates states whose energies vary significantly within the uncertainty range of the measured resonance position in Ref. [33].

Exact counting of the remaining particles after Rydberg excitation reveals the loss dynamics. In Fig. 2(c) we tune the laser to the $v = 0$ peak and measure particle loss over time. We observe significant pair loss but no apparent single-particle loss, suggesting that molecule loss involves a process ejecting both Rb and Cs from the tweezer, likely due to radiative decay. This decay converts molecular binding energy into kinetic energy that exceeds the tweezer depth, causing pair loss. Additionally, we observe that the line shape of the $v = 0$ feature in Fig. 2(b) is asymmetric and significantly broader than expected [39]. The cause remains unclear but persists for all molecular resonances observed at 4.78 G in the same tweezer.

In Fig. 2(d) we show the measured binding energies of $v = 0$ states for all nS ULRMs explored in this Letter. The empty triangles show theoretical predictions [39] that are in excellent agreement with the measured binding energies. This agreement spans more than one order of magnitude in energy and is achieved without fitting any parameters to our experimental data.

Next, we investigate the influence of the tweezers on the formation of ULRMs. Figure 3 shows how the tweezer intensity affects molecules in the ground vibrational state

$v = 0$ of the PEC, which approaches $|36S_{1/2}, m_j = -1/2\rangle_{\text{Rb}}$ asymptotically. In Fig. 3(a) we observe that higher tweezer intensity increases the transition frequency. This transition shift results from the differential ac Stark shift $\propto (\alpha_{\text{Rb+Cs}} - \alpha_v)I$, where $\alpha_{\text{Rb+Cs}}$ and α_v are the polarizability of the atom pair in $|g\rangle_{\text{Rb}}|g\rangle_{\text{Cs}}$ and the ULRM in state v , respectively. This measured shift is identical to that measured for the atomic transition $|g\rangle_{\text{Rb}} \rightarrow |r\rangle_{\text{Rb}}$ [39], indicating that tweezer intensity does not affect the ULRM's binding energy. Therefore, the molecular polarizability is the sum of the polarizabilities of the constituent particles, $\alpha_v = \alpha_{\text{Cs}} + \alpha_{\text{Rb}}$. At our tweezer wavelength, this implies a polarizability of $\alpha_v = 613 \times 4\pi\epsilon_0 a_0^3$, indicating the ULRMs are trapped.

The tweezer intensity also alters the probability of exciting the atoms to the molecular state, as seen by the changing peak heights in Fig. 3(a) for a fixed Rydberg pulse duration. Figure 3(b) shows pair loss as a function of pulse duration for three different intensities, with the laser tuned to the shifted molecular transition for each intensity. We fit the data to an exponential model, extracting the loss rate Γ_{PA} [39]. The changing loss rate as a function of tweezer intensity can be understood by considering the FCF f_v that dictates the coupling to the molecular state. The FCF is determined by the wave function overlap between the molecule and atom pair. In Fig. 3(c), we plot the radial probability density of the rovibrational ground state $v = 0$, which is strongly peaked around 100 nm. The green and orange curves depict the isotropic component of the wave function for an atom pair trapped in an anisotropic tweezer potential [39]. Increasing I from 2.2 kW/cm^2 (green) to 586 kW/cm^2 (orange) shifts the peak density to smaller R while narrowing its spread. In Fig. 3(d) we plot f_v^2 for our experimental parameters. The predicted FCF peaks at 6% around an intensity of 200 kW/cm^2 . For larger intensities, we can reach the regime where the atom pair's

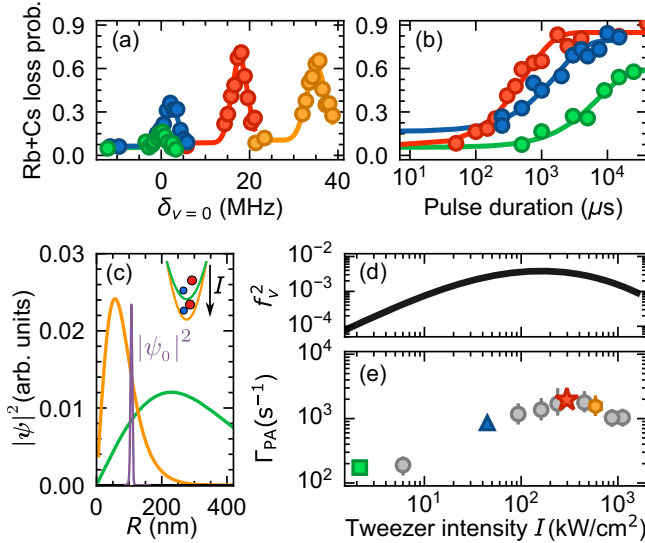


FIG. 3. (a) Probability of losing a Rb + Cs atom pair as a function of the two-photon detuning from the molecular state $v = 0$ at zero tweezer intensity $\delta_{v=0}$. The different colors represent spectra obtained at different tweezer intensities 2.2 kW/cm² (green), 45 kW/cm² (blue), 297 kW/cm² (red), and 586 kW/cm² (orange), respectively. (b) Atom-pair loss as a function of Rydberg pulse duration on resonance with the molecular state. The colors correspond to the same tweezer intensities as in (a) and the solid lines are fits to the experimental data [39]. (c) Probability density for the $v = 0$ molecular state $|\psi_0|^2$ (purple) and the ground-state atom pair (green and orange). The atom-pair wave functions show the projection of the cylindrical wave function onto the $\tilde{l} = 0, m_{\tilde{l}} = 0$ spherical harmonic [39], with colors corresponding to the same tweezer intensities as above. (d) The black line shows f_v^2 , the Franck-Condon factor squared, as a function of the tweezer intensity I . (e) Measured atom-pair loss rates Γ_{PA} as a function of the tweezer intensity. Colored markers correspond to the same tweezer intensities as in (a); gray markers show additional intensities omitted in (a) for clarity.

most likely separation shifts to distances smaller than the molecular bond length, as shown by the orange curve in Fig. 3(c). In Fig. 3(e) we plot the loss rate extracted from the measurements in Fig. 3(b). As the coupling to the molecular state is $\Omega_v \propto f_v$, we expect the measured atom pair loss rate is $\Gamma_{\text{PA}} \propto f_v^2$ [39]. The experimental data matches the predicted behavior well and we observe an order of magnitude increase in the loss rate for intensities between 200 and 600 kW/cm².

Controlling the FCF between the atom pair and ULRMs using the trap intensity provides a valuable experimental tool, previously limited to optical lattice experiments [9,67]. However, by trapping the atoms in the same tweezer we cannot decouple the most likely separation of the atom pair from the wave function spread. A key feature of the tweezer platform is the ability to reconfigure the array geometry, which we now exploit to position the atom pair at the separation required to maximize the FCF.

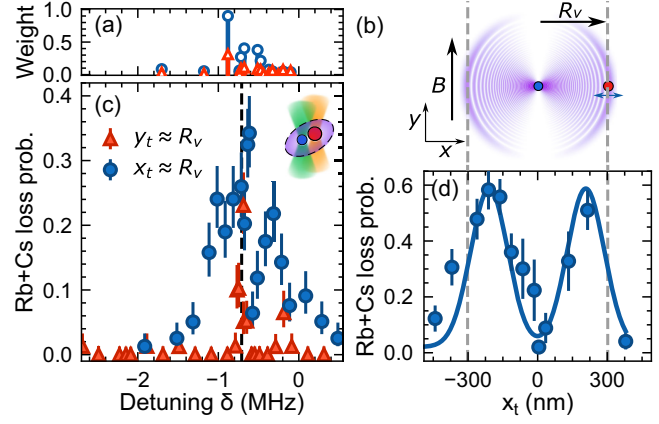


FIG. 4. Assembly of ULRMs in separate tweezers. (a) Blue circles (red triangles) show theoretical predictions for line strengths and positions for tweezers separated by the bond length $R_v = 300$ nm along the x axis (y axis). (b) The electron probability density of the state $|56D_{5/2}, m_j = 5/2\rangle_{\text{Rb}}$. A 4.78 G magnetic field B is applied along the y axis. The dashed lines show the calculated bond length $R_v = 300$ nm of the state $v = 0$. (c) Pair loss probability as a function of detuning δ from the atomic state $|56D_{5/2}, m_j = 5/2\rangle_{\text{Rb}}$. The Rb and Cs atoms are trapped in distinct tweezers (wavelengths 817 and 1066 nm, respectively), separated by 300 nm along x (blue) or y (red). (d) Pair loss probability as a function of the separation x_t of the 817 and 1066 nm tweezers along the x axis. The two-photon detuning is resonant with the loss feature indicated by the black dashed line in (c) and the solid blue line shows a double Gaussian fit to the experimental data.

We demonstrate the preparation of an ULRM across two separate tweezers in Fig. 4. Here, we retain Rb in the 817 nm tweezer. The relative separation of the two tweezers is tuneable in all three dimensions, with a positional resolution of approximately 50 nm in the $x - y$ plane [Fig. 4(b)] and 100 nm in the $x - z$ plane, limited by shot-to-shot fluctuations in the relative position of the tweezers [68]. To increase the bond length R_v relative to this positional fluctuation, we explore ULRMs at higher n . Figure 4(b) shows the electron probability density for the atomic state $|56D_{5/2}, m_j = 5/2\rangle_{\text{Rb}}$. We utilize the anisotropic wave function of this D state to demonstrate the control over the constituent particles afforded by our approach. The PEC's depth reduces to zero when the atoms are oriented along the quantization axis [39], meaning there are no molecular bound states. Figure 4(a) shows theoretical predictions for line strengths and positions for tweezers separated by the bond length $R_v = 300$ nm along the x axis (blue circles) and y axis (red triangles). We predict the ratio of the FCFs between the parallel and perpendicular alignment is nonzero and approximately 0.3 [39], caused by the residual atom pair's wave function spread in the $x - z$ plane.

Figure 4(c) shows spectroscopy of ULRMs below the atomic state $|56D_{5/2}, m_j = 5/2\rangle_{\text{Rb}}$. The blue (red) markers show data obtained with the tweezers separated by

approximately the bond length and oriented perpendicular (parallel) to the applied magnetic field. The measured spectrum exhibits a clear contrast between the two orientations and is in good agreement with our theoretical predictions.

In Fig. 4(d) we investigate how the coupling to the molecular state depends on the tweezer separation. We fix the detuning on resonance with the molecular line [dashed line in Fig. 4(c)] and orient the atom pair along the x axis, perpendicular to both the quantization axis and the tweezer propagation direction. We observe a striking dependence of atom loss on tweezer position, with a peak in the loss occurring when the Cs atom is positioned on either side of the Rb atom. Fitting the data with a double Gaussian, we extract an average displacement from the center of 210(10) nm. To compare with the expected bond length, we must account for the difference between the tweezer separation and the atomic separation, arising from the distinct atomic polarizabilities. For instance, the Cs atom is repelled by the 817 nm tweezer, increasing the atomic separation relative to the tweezer separation [69]. Numerical simulations of the tweezer potential [39] indicate that a tweezer separation of $x_t = 210$ nm corresponds to an atomic separation of $R = 300$ nm, consistent with the expected bond length.

Our demonstrated manipulation of the initial atom-pair state is promising for the realization of other forms of ULRMs such as giant polyatomic Rydberg molecules [70], which could be realized by combining diatomic molecules with Rydberg atoms [71,72]. Trapping of the constituent particles in separate tweezers bypasses problems with preparing atoms and molecules in the same trap [73] and can enhance the coupling to molecular states. This approach enables the selective preparation of different molecular symmetry groups and exotic molecular states based on the initial atom geometry [18], and opens up the possibility of manipulating ULRMs using tweezers. Importantly, our method is readily extendable to homonuclear systems [39], facilitating studies of both well-established and novel molecular species.

In conclusion, we have presented a new approach to studying ULRMs using optical tweezers, reporting the formation and characterization of individual Rb*Cs ULRMs. By leveraging the inherent single-particle manipulation of our approach, we have demonstrated control over the atom pair's relative wave function, optimizing the coupling to molecular states and achieving molecular association with atoms trapped in separate tweezers.

Our approach opens new pathways for exploring polyatomic ULRMs in programmable geometries and enables trapping of ULRMs for coherent control. Moreover, extending this method to other Rydberg tweezer platforms will expand the range of molecular species that can be studied and create new opportunities for integrating ULRMs into quantum simulation and computation platforms.

Acknowledgments—We thank M. P. A. Jones for helpful discussions. A. D. and M. E. thank F. Hummel for assistance with the magnetic field interaction. We acknowledge support from UK Research and Innovation (UKRI) Frontier Research Grant EP/X023354/1, the Royal Society, and Durham University.

A. G. and M. T. E. conceptualized the work; A. G. and T. R. H. performed the experiments; D. K. R. contributed to the experimental apparatus; A. A. T. D. and M. T. E. performed the theoretical work; S. L. C. supervised the experimental work. A. G. wrote the manuscript with contributions from all authors.

Data availability—The data that support the findings of this article are openly available [74].

-
- [1] S. L. Cornish, M. R. Tarbutt, and K. R. A. Hazzard, Quantum computation and quantum simulation with ultracold molecules, *Nat. Phys.* **20**, 730 (2024).
 - [2] D. DeMille, N. R. Hutzler, A. M. Rey, and T. Zelevinsky, Quantum sensing and metrology for fundamental physics with molecules, *Nat. Phys.* **20**, 741 (2024).
 - [3] T. Langen, G. Valtolina, D. Wang, and J. Ye, Quantum state manipulation and science of ultracold molecules, *Nat. Phys.* **20**, 702 (2024).
 - [4] C. Fey, F. Hummel, and P. Schmelcher, Ultralong-range Rydberg molecules, *Mol. Phys.* **118**, e1679401 (2019).
 - [5] M. T. Eiles, Trilobites, butterflies, and other exotic specimens of long-range Rydberg molecules, *J. Phys. B* **52**, 113001 (2019).
 - [6] F. Dunning, S. Kanungo, and S. Yoshida, Ultralong-range Rydberg molecules, *J. Phys. B* **57**, 212002 (2024).
 - [7] J. P. Shaffer, S. T. Rittenhouse, and H. R. Sadeghpour, Ultracold Rydberg molecules, *Nat. Commun.* **9**, 1965 (2018).
 - [8] H. Saßmannshausen and J. Deiglmayr, Observation of Rydberg-atom macrodimers: Micrometer-sized diatomic molecules, *Phys. Rev. Lett.* **117**, 083401 (2016).
 - [9] S. Hollerith, J. Zeiher, J. Rui, A. Rubio-Abadal, V. Walther, T. Pohl, D. M. Stamper-Kurn, I. Bloch, and C. Gross, Quantum gas microscopy of Rydberg macrodimers, *Science* **364**, 664 (2019).
 - [10] S. Hollerith, J. Rui, A. Rubio-Abadal, K. Srakaew, D. Wei, J. Zeiher, C. Gross, and I. Bloch, Microscopic electronic structure tomography of Rydberg macrodimers, *Phys. Rev. Res.* **3**, 013252 (2021).
 - [11] T. Manthey, T. Niederprüm, O. Thomas, and H. Ott, Dynamically probing ultracold lattice gases via Rydberg molecules, *New J. Phys.* **17**, 103024 (2015).
 - [12] J. D. Whalen, S. K. Kanungo, Y. Lu, S. Yoshida, J. Burgdörfer, F. B. Dunning, and T. C. Killian, Heteronuclear Rydberg molecules, *Phys. Rev. A* **101**, 060701(R) (2020).
 - [13] M. Peper and J. Deiglmayr, Heteronuclear long-range Rydberg molecules, *Phys. Rev. Lett.* **126**, 013001 (2021).
 - [14] M. Peper, M. Trautmann, and J. Deiglmayr, Role of Coulomb antiblockade in the photoassociation of long-range Rydberg molecules, *Phys. Rev. A* **107**, 012812 (2023).

- [15] F. Hummel, P. Schmelcher, H. Ott, and H. R. Sadeghpour, An ultracold heavy Rydberg system formed from ultra-long-range molecules bound in a stairwell potential, *New J. Phys.* **22**, 063060 (2020).
- [16] M. Peper and J. Deiglmayr, Formation of ultracold ion pairs through long-range Rydberg molecules, *J. Phys. B* **53**, 064001 (2020).
- [17] M. Khazali and W. Lechner, Scalable quantum processors empowered by the Fermi scattering of Rydberg electrons, *Commun. Phys.* **6**, 57 (2023).
- [18] M. T. Eiles, J. Pérez-Ríos, F. Robicheaux, and C. H. Greene, Ultracold molecular Rydberg physics in a high density environment, *J. Phys. B* **49**, 114005 (2016).
- [19] M. T. Eiles, A. Eisfeld, and J. M. Rost, Anderson localization of a Rydberg electron, *Phys. Rev. Res.* **5**, 033032 (2023).
- [20] M. T. Eiles, C. W. Wächtler, A. Eisfeld, and J. M. Rost, Topological edge states in a Rydberg composite, *Phys. Rev. B* **109**, 075422 (2024).
- [21] A. M. Kaufman and K.-K. Ni, Quantum science with optical tweezer arrays of ultracold atoms and molecules, *Nat. Phys.* **17**, 1324 (2021).
- [22] L. R. Liu, J. D. Hood, Y. Yu, J. T. Zhang, N. R. Hutzler, T. Rosenband, and K.-K. Ni, Building one molecule from a reservoir of two atoms, *Science* **360**, 900 (2018).
- [23] R. V. Brooks, S. Spence, A. Guttridge, A. Alampounti, A. Rakonjac, L. A. McArd, J. M. Hutson, and S. L. Cornish, Preparation of one ^{87}Rb and one ^{133}Cs atom in a single optical tweezer, *New J. Phys.* **23**, 065002 (2021).
- [24] K. Singh, S. Anand, A. Pocklington, J. T. Kemp, and H. Bernien, Dual-element, two-dimensional atom array with continuous-mode operation, *Phys. Rev. X* **12**, 011040 (2022).
- [25] W. B. Cairncross, J. T. Zhang, L. R. B. Picard, Y. Yu, K. Wang, and K.-K. Ni, Assembly of a rovibrational ground state molecule in an optical tweezer, *Phys. Rev. Lett.* **126**, 123402 (2021).
- [26] D. K. Ruttley, A. Guttridge, T. R. Hepworth, and S. L. Cornish, Enhanced quantum control of individual ultracold molecules using optical tweezer arrays, *PRX Quantum* **5**, 020333 (2024).
- [27] I. I. Beterov and M. Saffman, Rydberg blockade, Förster resonances, and quantum state measurements with different atomic species, *Phys. Rev. A* **92**, 042710 (2015).
- [28] S. Anand, C. E. Bradley, R. White, V. Ramesh, K. Singh, and H. Bernien, A dual-species Rydberg array, *Nat. Phys.* **20**, 1744 (2024).
- [29] C. H. Greene, A. S. Dickinson, and H. R. Sadeghpour, Creation of polar and nonpolar ultra-long-range Rydberg molecules, *Phys. Rev. Lett.* **85**, 2458 (2000).
- [30] E. Fermi, On the pressure-induced displacement of the elevated lines of spectral series, *Nuovo Cimento* **11**, 157 (1934).
- [31] A. A. Khuskivadze, M. I. Chibisov, and I. I. Fabrikant, Adiabatic energy levels and electric dipole moments of Rydberg states of Rb_2 and Cs_2 dimers, *Phys. Rev. A* **66**, 042709 (2002).
- [32] E. L. Hamilton, C. H. Greene, and H. Sadeghpour, Shape-resonance-induced long-range molecular Rydberg states, *J. Phys. B* **35**, L199 (2002).
- [33] M. Scheer, J. Thøgersen, R. C. Bilodeau, C. A. Brodie, H. K. Haugen, H. H. Andersen, P. Kristensen, and T. Andersen, Experimental evidence that the $6s6p\ ^3P_j$ states of Cs^- are shape resonances, *Phys. Rev. Lett.* **80**, 684 (1998).
- [34] M. T. Eiles and C. H. Greene, Hamiltonian for the inclusion of spin effects in long-range Rydberg molecules, *Phys. Rev. A* **95**, 042515 (2017).
- [35] F. Hummel, C. Fey, and P. Schmelcher, Spin-interaction effects for ultralong-range Rydberg molecules in a magnetic field, *Phys. Rev. A* **97**, 043422 (2018).
- [36] F. Hummel, C. Fey, and P. Schmelcher, Alignment of s -state Rydberg molecules in magnetic fields, *Phys. Rev. A* **99**, 023401 (2019).
- [37] C. H. Greene and M. T. Eiles, Green's-function treatment of Rydberg molecules with spins, *Phys. Rev. A* **108**, 042805 (2023).
- [38] H. Saßmannshausen, F. Merkt, and J. Deiglmayr, Experimental characterization of singlet scattering channels in long-range Rydberg molecules, *Phys. Rev. Lett.* **114**, 133201 (2015).
- [39] See Supplemental Material at <http://link.aps.org/supplemental/10.1103/PhysRevLett.134.133401> for details of theoretical calculations of molecular potentials, bound states, and Franck-Condon factors, the experimental apparatus, light shift measurements, observations of line broadening, modeling of the tweezer separation, and applicability of our approach to other systems, which includes Refs. [40–66].
- [40] N. Šibalić, J. D. Pritchard, C. S. Adams, and K. J. Weatherill, ARC: An open-source library for calculating properties of alkali Rydberg atoms, *Comput. Phys. Commun.* **220**, 319 (2017).
- [41] A. Omont, On the theory of collisions of atoms in Rydberg states with neutral particles, *J. Phys.* **38**, 1343 (1977).
- [42] C. Fey, M. Kurz, P. Schmelcher, S. T. Rittenhouse, and H. R. Sadeghpour, A comparative analysis of binding in ultralong-range Rydberg molecules, *New J. Phys.* **17**, 055010 (2015).
- [43] F. Engel, T. Dieterle, F. Hummel, C. Fey, P. Schmelcher, R. Löw, T. Pfau, and F. Meinert, Precision spectroscopy of negative-ion resonances in ultralong-range Rydberg molecules, *Phys. Rev. Lett.* **123**, 073003 (2019).
- [44] C. Bahrim and U. Thumm, Low-lying $^3P^o$ and $^3S^e$ states of Rb^- , Cs^- , and Fr^- , *Phys. Rev. A* **61**, 022722 (2000).
- [45] M. Peper and J. Deiglmayr, Heteronuclear long-range Rydberg molecules, *Phys. Rev. Lett.* **126**, 013001 (2021).
- [46] C. Bahrim, U. Thumm, and I. Fabrikant, $^3S^e$ and 1S_e scattering lengths for $e^- + \text{Rb}$, Cs and Fr collisions, *J. Phys. B* **34**, L195 (2001).
- [47] H. Saßmannshausen, J. Deiglmayr, and F. Merkt, Long-range Rydberg molecules, Rydberg macrodimers and Rydberg aggregates in an ultracold Cs gas: Investigation of long-range interactions between atoms in electronically highly excited states, *Eur. Phys. J. Special Topics* **225**, 2891 (2016).
- [48] O. I. Tolstikhin, V. N. Ostrovsky, and H. Nakamura, Siegert pseudostate formulation of scattering theory: One-channel case, *Phys. Rev. A* **58**, 2077 (1998).
- [49] A. A. Durst, M. Simić, N. Abraham, and M. T. Eiles, Non-adiabatic couplings as a stabilization mechanism in long-range Rydberg molecules, [arXiv:2408.14919](https://arxiv.org/abs/2408.14919).

- [50] V. Bendkowsky, B. Butscher, J. Nipper, J. B. Balewski, J. R. Shaffer, R. Löw, T. Pfau, W. Li, J. Stanojevic, T. Pohl, and J. M. Rost, Rydberg trimers and excited dimers bound by internal quantum reflection, *Phys. Rev. Lett.* **105**, 163201 (2010).
- [51] A. T. Krupp, A. Gaj, J. B. Balewski, P. Ilzhöfer, S. Hofferberth, R. Löw, T. Pfau, M. Kurz, and P. Schmelcher, Alignment of d -state Rydberg molecules, *Phys. Rev. Lett.* **112**, 143008 (2014).
- [52] F. Böttcher, A. Gaj, K. M. Westphal, M. Schlagmüller, K. S. Kleinbach, R. Löw, T. C. Liebisch, T. Pfau, and S. Hofferberth, Observation of mixed singlet-triplet Rb_2 Rydberg molecules, *Phys. Rev. A* **93**, 032512 (2016).
- [53] A. Ciamei, A. Bayerle, C.-C. Chen, B. Pasquiou, and F. Schreck, Efficient production of long-lived ultracold Sr_2 molecules, *Phys. Rev. A* **96**, 013406 (2017).
- [54] T. Tomita, S. Nakajima, I. Danshita, Y. Takasu, and Y. Takahashi, Observation of the Mott insulator to superfluid crossover of a driven-dissipative Bose-Hubbard system, *Sci. Adv.* **3**, e1701513 (2017).
- [55] S. Spence, R. V. Brooks, D. K. Ruttley, A. Guttridge, and S. L. Cornish, Preparation of ^{87}Rb and ^{133}Cs in the motional ground state of a single optical tweezer, *New J. Phys.* **24**, 103022 (2022).
- [56] H. Jeffreys, An invariant form for the prior probability in estimation problems, *Proc. R. Soc. A* **186**, 453 (1946).
- [57] L. D. Brown, T. T. Cai, and A. DasGupta, Interval estimation for a binomial proportion, *Stat. Sci.* **16**, 101 (2001).
- [58] T. T. Cai, One-sided confidence intervals in discrete distributions, *J. Stat. Plann. Infer.* **131**, 63 (2005).
- [59] P. Barakhshan, A. Marrs, A. Bhosale, B. Arora, R. Eigenmann, and M. S. Safronova, Portal for high-precision atomic data and computation (version 2.0) [Online] (2022), <https://www.udel.edu/atom/>.
- [60] S. Hollerith, V. Walther, K. Srakaew, D. Wei, D. Adler, S. Agrawal, P. Weckesser, I. Bloch, and J. Zeiher, Rydberg molecules bound by strong light fields, *PRX Quantum* **5**, 030335 (2024).
- [61] K. Wang, X. He, R. Guo, P. Xu, C. Sheng, J. Zhuang, Z. Xiong, M. Liu, J. Wang, and M. Zhan, Preparation of a heteronuclear two-atom system in the three-dimensional ground state in an optical tweezer, *Phys. Rev. A* **100**, 063429 (2019).
- [62] R. V. Brooks, A. Guttridge, M. D. Frye, D. K. Ruttley, S. Spence, J. M. Hutson, and S. L. Cornish, Feshbach spectroscopy of Cs atom pairs in optical tweezers, *New J. Phys.* **24**, 113051 (2022).
- [63] L. A. Reynolds, E. Schwartz, U. Ebling, M. Weyland, J. Brand, and M. F. Andersen, Direct measurements of collisional dynamics in cold atom triads, *Phys. Rev. Lett.* **124**, 073401 (2020).
- [64] L. Su, A. Douglas, M. Szurek, A. H. Hébert, A. Krahn, R. Groth, G. A. Phelps, O. Marković, and M. Greiner, Fast single atom imaging for optical lattice arrays, *Nat. Commun.* **16**, 1017 (2025).
- [65] L. Du, P. Barral, M. Cantara, J. de Hond, Y.-K. Lu, and W. Ketterle, Atomic physics on a 50-nm scale: Realization of a bilayer system of dipolar atoms, *Science* **384**, 546 (2024).
- [66] M. Weyland, S. S. Szigeti, R. A. B. Hobbs, P. Ruksasakchai, L. Sanchez, and M. F. Andersen, Pair correlations and photoassociation dynamics of two atoms in an optical tweezer, *Phys. Rev. Lett.* **126**, 083401 (2021).
- [67] O. Thomas, C. Lippe, T. Eichert, and H. Ott, Experimental realization of a Rydberg optical Feshbach resonance in a quantum many-body system, *Nat. Commun.* **9**, 2238 (2018).
- [68] A. Guttridge, D. K. Ruttley, A. C. Baldock, R. González-Férez, H. R. Sadeghpour, C. S. Adams, and S. L. Cornish, Observation of Rydberg blockade due to the charge-dipole interaction between an atom and a polar molecule, *Phys. Rev. Lett.* **131**, 013401 (2023).
- [69] D. K. Ruttley, A. Guttridge, S. Spence, R. C. Bird, C. R. Le Sueur, J. M. Hutson, and S. L. Cornish, Formation of ultracold molecules by merging optical tweezers, *Phys. Rev. Lett.* **130**, 223401 (2023).
- [70] S. T. Rittenhouse and H. R. Sadeghpour, Ultracold giant polyatomic Rydberg molecules: Coherent control of molecular orientation, *Phys. Rev. Lett.* **104**, 243002 (2010).
- [71] R. González-Férez, S. T. Rittenhouse, P. Schmelcher, and H. R. Sadeghpour, A protocol to realize triatomic ultralong range Rydberg molecules in an ultracold KRb gas, *J. Phys. B* **53**, 074002 (2020).
- [72] D. Mellado-Alcedo, A. Guttridge, S. L. Cornish, H. R. Sadeghpour, and R. González-Férez, Ultralong-range Cs-RbCs Rydberg molecules: Nonadiabaticity of dipole moments, *Phys. Rev. A* **110**, 013314 (2024).
- [73] P. D. Gregory, J. A. Blackmore, F. M. D, L. M. Fernley, S. L. Bromley, J. M. Hutson, and S. L. Cornish, Molecule-molecule and atom-molecule collisions with ultracold RbCs molecules, *New J. Phys.* **23**, 125004 (2021).
- [74] A. Guttridge, T. R. Hepworth, D. K. Ruttley, A. A. T. Durst, M. T. Eiles, and S. L. Cornish, Individual assembly of two-species Rydberg molecules using optical tweezers [dataset] (2024), [10.15128/r102870v96p](https://doi.org/10.15128/r102870v96p).